Kiloelectronvolt Argon-Induced Molecular Desorption from a Bulk Polystyrene Solid

Arnaud Delcorte*

PCPM, Universite Catholique de Louvain, 1 Croix du Sud, B1348, Louvain-la-Neuve, Belgium

Barbara J. Garrison

Department of Chemistry, The Pennsylvania State University, 152 Davey Lab, University Park, Pennsylvania 16802

Received: March 15, 2004

The particle-induced desorption of polystyrene (PS) tetramers from a molecular solid sample has been studied using molecular dynamics simulations. To identify the specifics of bulk organic sample sputtering better, a PS monolayer on silver and a "thick" (45 Å) PS sample have been bombarded by 0.5-keV Ar projectiles, at a polar angle of 45°. The sputtering yields of molecular species and their kinetic energy distributions were calculated from the final positions and velocities of the atoms in the simulation. One of the main results of this study is that the kinetic energy spectrum of ejected PS tetramers is significantly narrower for the bulk sample than the overlayer on metal. The results are explained in terms of energy transfer in the surface region. For the PS overlayer on silver, the sputtering process is characterized by the quick dissipation of the projectile energy in the metal substrate, accompanied by the fast ejection of molecules (1 ps) with a significant amount of kinetic energy. For the bulk sample, the sputtering process is slow (10 ps), the energy remains localized in the excited molecules (vibrations), and the resulting kinetic energies are comparatively low. Based on a limited series of trajectories using Ar projectiles excited at an accelerating voltage of 5 keV, we also comment on the effect of the primary particle energy on the molecular motion/desorption processes.

1. Introduction

In the past decade, molecular dynamics (MD) simulations have fueled a series of insightful studies regarding the elucidation of molecular desorption from organic overlayers on inorganic substrates.[1−3] In addition to their explanatory power, these simulations sometimes proved to be predictive, paving the way for new analytical developments. For instance, several interesting properties of fullerene projectile−surface interactions were theoretically investigated before such projectile sources were available.[4] Currently, many application fields of particle-induced desorption mass spectrometries—in particular, secondary ion mass spectrometry (SIMS)—involve thick organic samples, e.g., polymer films, molecular multilayers, analyte molecules in a liquid matrix (fast atom bombardment mass spectrometry), protein coatings, cells, and tissues.[5] However, molecular desorption from thick samples has been much less explored theoretically, because of the lack of adequate empirical potentials and the huge amount of computer processing unit (CPU) time needed to compute such systems.

Prior to the first attempts at modeling organic sample sputtering via MD simulations, several analytical models had been proposed to explain the emission of large molecular ensembles by mechanisms involving collective atomic motions in the target. They were developed to overcome the evident inadequacy of the binary atomic collision theory[6] (or direct electronic excitations under MeV ion irradiation) to describe the emission of large material clusters and biomolecules in keV and MeV ion bombardment. The concept behind these theoretical approaches is that such polyatomic ensembles and intact molecules can only emerge from regions where many atoms move in a concerted fashion. According to the models, these collective effects result from the fast conversion of electronic and/or collisional interactions into large-scale correlated motion. In addition to the thermal and energy spike[7−9] models, the gas-flow,[10,11] shock-wave,[12−16] and pressure-pulse[17] models constitute the most achieved efforts at rationalizing the aforementioned concept, using slightly different premises and approximations. In addition to the sputtering of metals[18−20] and condensed amorphous rare gases,[21] these models were applied with some success to organic samples,[22] including biomolecules.[23−25] However, detailed experimental observations (kinetic energy distributions, angular distributions) are still scarce, and the theoretical predictions often seem to be too ambiguous for these models to be definitely validated in the case of keV particle-induced desorption.

In the MD simulation arena, early reports investigated the electronic[26] and nuclear sputtering[27] of bulk molecular solids, using a coarse-grained representation of the sample (spheres bound by a Lennard-Jones (LJ) potential). In the MeV ion-induced desorption report,[26] the molecules in the irradiation track were forced to expand in a popcorn-like manner,[28] causing surface disruption and molecular ejection. The emission yields and angular distributions of molecules were predicted. In the nuclear sputtering regime,[27] the temperature-versus-time profile of the two-dimensional LJ matrix, after 200-eV projectile bombardment, was interpreted in terms of shock wave, spinodal transition, and cluster relaxation. Among the pioneers of atomistic MD simulation of organic solids were Beardmore and Smith, who modeled a polyethylene crystal under 1-keV Ar-ion bombardment, using the Brenner reactive potential for

* Author to whom correspondence should be addressed. Telephone: 32-10-473582. Fax: 32-10-473452. E-mail address: delcorte@pcpm.ucl.ac.be.

10.1021/jp0402131 CCC: $27.50
Published on Web 09/14/2004

hydrocarbons.[29] Their study identified different types of particle-induced damage in the solid (chain scission, cross-linking, and carbonization) and the ejection process could be split in two batches: a quick sputtering of atoms and radicals, followed by a slower desorption of larger molecular segments. However, the model did not take into account attractive forces between neighboring chain segments. A study by Nordlund et al., using the same potential, also identified an interesting chemical sputtering process for C atoms that occurs when a "slow" (1−30 eV) H atom interacts with a C−C bond.[30] More theoretical studies are emerging in the recent literature, because of the advent of an improved hydrocarbon potential including intermolecular forces.[31] This potential was first used to investigate the sputtering of a crystal of benzene.[32] The results suggested the concept of molecular collision cascade, by analogy to the atomic collision cascade observed in inorganic materials. Our recent work analyzed the desorption of kDa molecules embedded in a low-molecular-weight matrix.[33] Some major mechanisms were delineated, such as vibrational emission and cluster desolvation; however, an exhaustive analysis of the detailed mechanisms would have required a larger sample.

For the present study, we designed an organic sample that is significantly larger than the average volume disturbed by 500-eV Ar atoms (250 nm^3 versus 40 nm^3, in ref 33) and can absorb that amount of energy without decomposing. This sample is a homogeneous, amorphous solid that is composed of polystyrene (PS) molecules. PS tetramers (474 Da) have been chosen for several reasons. First, their mass and size correspond to a category of molecules that form molecular solids at room temperature and are therefore of analytical interest. Second, even though they do not contain heteroatoms (adequate empirical potentials do not exist), they exhibit specific chemical features (phenyl rings, butyl endgroups). Third, with their flexible hydrocarbon backbone, they are expected to display some of the properties of polymers (motion of chain segments, entanglement). With respect to the "matrix" samples of ref 33, it should be more strongly bound, because the molecules are somewhat entangled and their contact surface is larger. Finally, because of the choice of PS tetramer building blocks, the results can be easily compared to previous reports using the same molecule deposited as a monolayer on a metal surface.[34,35]

One of the main results of this work concerns the kinetic energy distributions of PS tetramers desorbed from a molecular sample under 500-eV Ar oblique incidence. The comparison shows that it is significantly narrower than that of molecules ejected from a molecular submonolayer on metal under the same incidence. This result is analyzed in terms of energy-transfer considerations, using the microscopic insights provided by the MD simulations. The bombardment of molecular solids by 5-keV Ar projectiles, which is a situation more often encountered in analytical instruments, is also critically discussed on the basis of a limited series of trajectories computed with our PS tetramer sample.

2. Computational Method

MD simulations have been chosen to model the keV particle-induced desorption of short PS tetramers (four repeat units) from a bulk PS sample. The details of the simulation scheme are described elsewhere.[34,36] During the course of these simulations, Hamilton's equations of motion are integrated over some time interval to determine the position and velocity of each particle as a function of time.[37,38] The energy and forces in the system are described by many-body interaction potentials. The C−C, C−H, and H−H interactions are described by the AIREBO

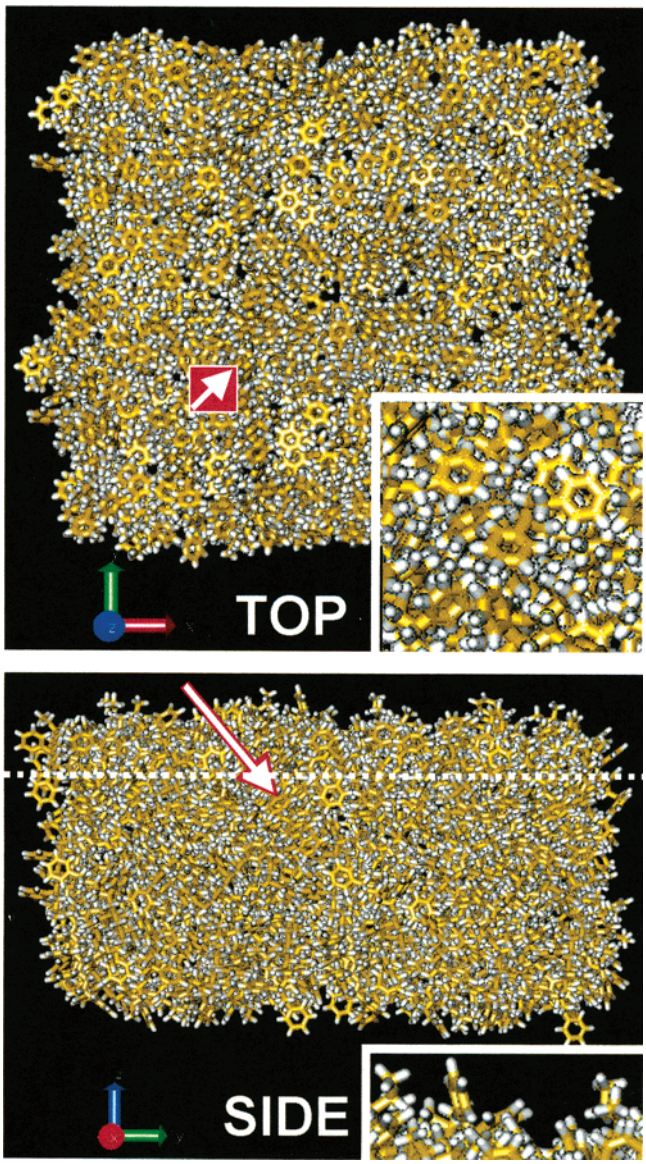

Figure 1. Top and side views of the computational cell of sample B. Insets show close-up views of the sample surface. The impact area is indicated by a red rectangle in the top view of the sample, and the white arrows show the direction of the incoming projectiles.

potential.[31] This potential is based on the reactive empirical bond-order (REBO) potential developed by Brenner for hydrocarbon molecules[39−41] and includes nonbonding interactions through an adaptative treatment that conserves the reactivity of the REBO potential. The Ag−C and Ag−H interactions are described by pairwise additive LJ potential functions, with the parameters given in ref 33. To model the Ag−Ag interactions, we used the molecular dynamics/Monte Carlo corrected effective medium (MD/MC−CEM) potential for face-centered cubic (fcc) metals.[42] The Ar−C, Ar−H, and Ar−Ag interactions are described by purely repulsive Molière potential functions.

The computational cell is a box containing 18 096 atoms, forming 232 PS molecules (Figure 1). The total size of the molecular sample was chosen according to preliminary calculations (1000 trajectories) of atom ranges in a C,H (1:1)-containing solid, using the TRIM program.[43,44] The adequacy of the sample size for the selected projectile energy was confirmed afterward by the results of the MD simulations. The final sample was obtained after many stages of clustering and relaxation within finite boundaries. In the clustering stages, a small downward

velocity was given to an ensemble of noninteracting molecules initially located above the sample, so that they aggregate/accumulate in the predefined box. In the relaxation stages, a temperature of 150 K was applied for at least 10 ps, allowing the molecules to rearrange in the box. After completion of this procedure, the entire sample was allowed to relax once again, for ~100 more ps and without any constraint on the boundaries. As a result, the free-evolving sample slightly deformed and gained a significant surface roughness (see inset of Figure 1b). This final relaxation step was considered necessary because open boundary conditions are used for the simulation of sputtering.[45] The inset of Figure 1a provides a close-up view of the molecules intermingled in the surface region. The binding energy of a molecule in the bulk of the sample is 2.3 eV. It was calculated as the difference between (i) the total energy of the final sample and (ii) the sum of the energy of the molecule (isolated from the sample) plus the energy of the sample without that specific molecule.

For the sputtering study, 500-eV incident Ar atoms were selected, which is consistent with previous studies. An incident polar angle of 45° (signified by the white arrow in Figure 1b) was selected to mimic the usual experimental conditions. To extend the "apparent depth" of the sample in the direction of the projectiles, we opted for an azimuthal angle of 45° (denoted by the white arrow in Figure 1a) and a target area that was moved away from the center toward the projectile starting positions above the sample (see red square in Figure 1a). This is an adequate choice to keep the action of a large majority of the trajectories in the central region of the samples, as is shown in the Results section. The aiming points were uniformly distributed in the target area. Two hundred trajectories were computed with this sample, for a total running time of 10 ps each.

For comparison purpose, 800 trajectories were calculated using a second sample, consisting of an overlayer of PS oligomers on a flat silver substrate (see Figure 1 in ref 46). This sample, which was designed during the course of a previous study, was relaxed within the AIREBO potential. Ar projectiles accelerated at 500 eV, with 45° polar and azimuthal angles, were directed at the sample surface and the ejected species were counted after 10 ps.

At the end of each trajectory, atoms that had a velocity vector directed away from the surface and were at a height of at least 8 Å above the top of the sample were considered as sputtered atoms. For identifying clusters, pairs of atoms were checked to see if there was an attractive interaction between them, in which case they were considered linked.[47,48] If the total internal energy of such a linked group of atoms was less than zero, then it was considered to be an ejected molecule. In all the simulations, the mass of hydrogen was taken to be that of tritium (3 amu), to increase computational efficiency.[36] Experimentally observable properties, such as total yield, yield distribution, and kinetic energy were calculated from the final positions, velocities, and masses of all the ejected species. Mechanistic information was obtained by monitoring the time evolution of relevant collisional events.

3. Results and Discussion

This study aims at unraveling the physics that governs molecular emission from bulk organic samples bombarded by energetic projectiles. To emphasize the specific processes at play, the results involving the molecular sample depicted in Figure 1 (sample B) are compared to those obtained from a monolayer of PS tetramers deposited on silver (sample L), under the same bombardment conditions. A picture of this monolayer system is shown in Figure 1 in ref 46. In addition to the projectile properties, another difference between our new calculations with sample L and the calculations described in ref 46 is that the results presented hereafter have been obtained using the AIREBO potential, i.e., intermolecular forces were taken into account. After a brief presentation of a characteristic desorption event from the molecular sample, the discussion compares the emission statistics of samples B and L. The results are explained using a visualization of the energy transfer in the surface layer of both samples for characteristic trajectories, leading to the ejection of intact molecules. Finally, we discuss the validity of our observations for the high-energy (5-keV) bombardment of molecular samples.

3.1. Ejection Dynamics. One advantage of the MD approach is that it provides direct insights in the microscopic processes at play, e.g., the dynamics of a set of molecules perturbed by an energetic projectile, through the visualization of the trajectory movies. Such snapshots of a sputtering event inducing molecular ejection are shown as examples in Figure 2. They serve as a guide for further analysis.

The situation after 2 ps is displayed in Figure 2, first frame. A few H atoms have already left the frame and another one is departing the sample. The solid appears almost undisturbed, except for some slow upward molecular motion at the top surface. Note that, at this time, the ejection process would be already over for most samples consisting of an organic monolayer on an inorganic substrate, including sample L in our study. After 4 ps (second frame), the upward motion of a group of surface molecules, accompanied by one C_2H fragment (right inset), is obvious. Some molecules also protrude in the bottom of the sample; however, they are unable to escape the solid. An acetylene fragment leaves through that side of the computation cell (left inset). At the end of the trajectory, three intact molecules are ejected, and those that once formed an intricate cluster (second frame) are now separate. Another molecule is hovering in the surface region, without sufficient energy for desorption.

The collision tree of the event, i.e., the successive positions of the moving atoms in the first 150 fs of the trajectory, is shown in the bottom frame of Figure 2. It is well-confined in the organic medium and splits in distinct branches at 8 Å under the surface. The atomic cascade terminates some 10−15 Å below. One branch intercepts the surface, leading to the fast ejection of a H atom, whereas the others dissipate their energy in the organic medium. The collision tree confirms that the choice of a sample this size is reasonable, with respect to the investigated processes. With a larger sample, the energy responsible for the motion at the bottom of the sample would probably be more realistically damped; however, it is unlikely that more ejection would occur under such 500-eV projectile impacts.

To summarize, Figure 2 shows that 500-eV Ar projectiles are able to initiate enough action in an organic sample surface to cause the ejection of several 0.5 kDa molecules in a single event. Generally, we observe a continuum of events, from no ejection to high ejection yields, and the depicted trajectory is representative of the upper 10% in terms of total ejected mass. The following subsection provides a more-detailed view of these statistics.

3.2. Ejection Statistics. Some important quantities regarding the ejected species are gathered in Table 1 for the two systems under investigation. The first series of values describes the statistics of molecular emission. The percentages of trajectories

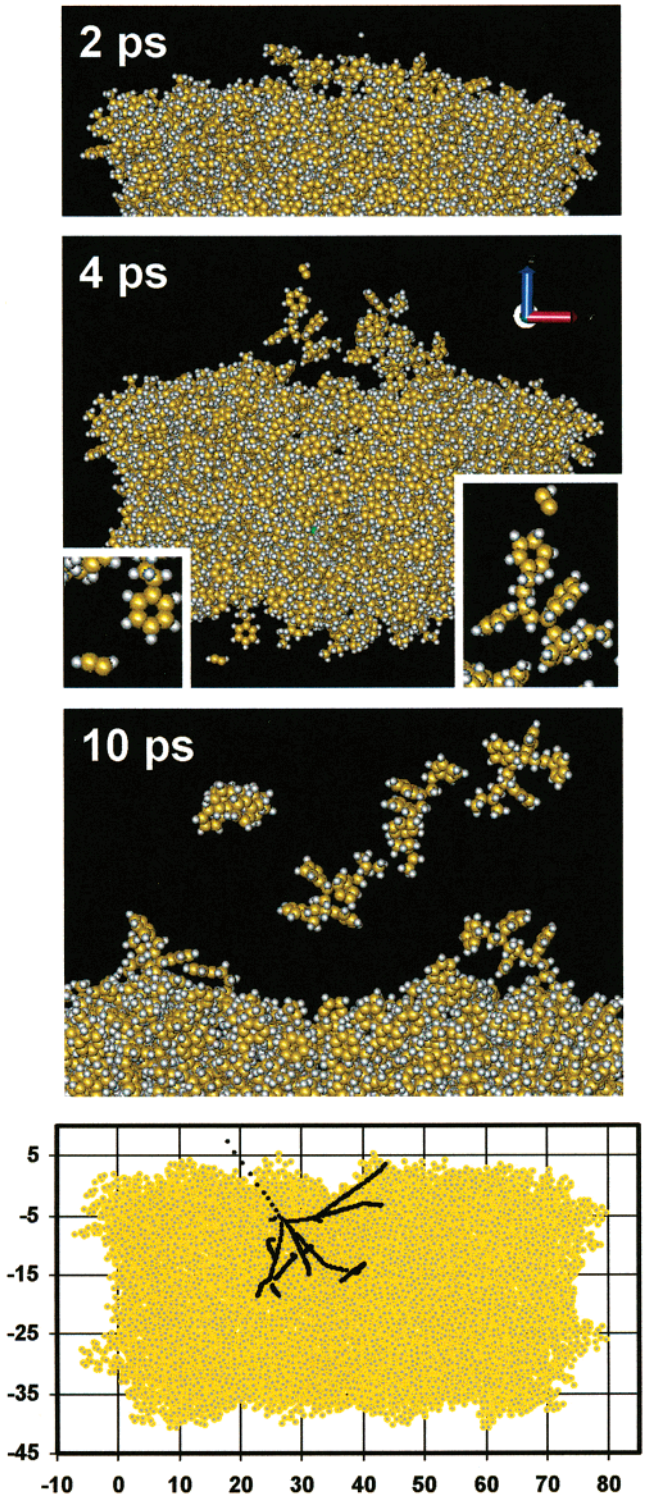

Figure 2. Sputtering sample B. Snapshots (2, 4, and 10 ps) of the time evolution of a characteristic trajectory showing the ejection of three intact molecules along with other fragments. The insets provide close-up views of details of interest for the discussion. The last frame of the figure is the collision tree of the atomic collision cascade. The sample is depicted by yellow-gray spheres, whereas the successive positions of atoms in the collision cascade are represented by black dots.

in which molecular emission is observed, and the corresponding emission yield, are split according to the number of ejected molecules per trajectory. The results show that half of the trajectories lead to molecular ejection with the bulk sample (B), versus one-fifth of the trajectories for the PS monolayer (sample L). As a result, molecular ejection is three times more probable with the bulk sample than the monolayer sample (see the yield column in Table 1). Dimer emission is observed only for the bulk sample. The second series of values concerns fragmentation. A similar number of trajectories (~50%) lead to the ejection of acetylene molecules (the most intense among small fragments) for both samples. In contrast, the percentage of trajectories leading to the desorption of PS molecules having lost an H atom and the related yield are four times larger with the bulk sample. The difference is even more dramatic for recombination products (third series), which are not rare with the bulk sample. For instance, the addition of an H atom to an intact molecule is 30 times more probable with sample B and, with the addition of a larger molecular group, 6 times more probable. Note that the observed fragmentation and recombination yields remain well below 1.

The case of H atom addition to form an M + H adduct might have implications for SIMS, where $(M + H)^+$ cations are commonly observed. In all the calculated trajectories where the M + H departs with a relatively low internal energy (a few eV), H addition is observed to occur in the para position of a phenyl residue belonging to the PS molecule. This structure is reported in the literature for $R-C_6H_6^+$ cations, and its formation enthalpy is relatively low, in comparison with other ionic isomers.[49] In the simulations, internally excited M + H adducts (>10 eV) present more-diverse structures, including bond scissions and rearrangements that also involve the phenyl rings. In that case, no rule could be established concerning the H-atom addition site.

The observation of a larger molecular yield with sample B deserves a comment. A similar conclusion has been reported from MD simulations of benzene multilayers, as compared to monolayers.[50] The underlying substrate, in that case, was shown to have a crucial role in the calculated yields. Such an effect is definitely absent of our simulations. There are few experimental studies measuring the yield of neutral molecules both from monolayers and thick samples. Nevertheless, the trend of increasing the yield when going to thicker samples seems to be at odds with most of the experimental results recently published. For adenine under 10-keV Ar^+ bombardment,[51] and benzene[52,53] and phenol[53] under 8-keV Ar^+ bombardment, the maximum postionized neutral yield corresponds to the monolayer sample. The yield peaks at a higher coverage for β-alanine bombarded by 10-keV Ar^+ cations, which seems to be the only counterexample at this point.[54] In that particular case, the molecular ion $(M + H)^+$ yield maximizes around one monolayer, although the post-ionized neutral yield does not, which also shows that results involving neutrals cannot necessarily be generalized to ions in this matter. Because no report is available concerning neutral ejection from PS or similar samples, the results of our simulations remain to be verified experimentally.

Another physical quantity that can be experimentally measured is the kinetic energy of the ejected molecules, at least as a distribution. In Figure 3, we plot the kinetic energy distributions (KEDs) of PS molecules sputtered from samples B and L. Each point of the KEDs corresponds to the cumulated intensity in a 0.2-eV energy window around the nominal energy value, i.e., the error on the distribution widths (broadening) is of the order of 0.1 eV. The KED of PS oligomers sputtered from a monolayer adsorbed on silver (sample L, denoted by plus signs in Figure 3) is very similar to that previously reported for the same sample but with a different impact angle and without considering intermolecular forces in the system.[34] The difference of width between the result of ref 34 and the distribution of Figure 3 is mainly due to the different bandpass

TABLE 1: Statistics of the Sputtered Species for Sample L (800 Trajectories) and Sample B (200 Trajectories)

	Sample L		Sample B	
	% of trajectories	yield	% of trajectories	yield
molecular emission				
0 molecules	78.8	0.0	49.5	0.0
1 molecule	17.0	0.17	36.8	0.37
2 molecules	3.1	0.06	9.8	0.20
3 or more molecules	1.1	0.03	3.9	0.12
total	100.0	0.27	100.0	0.79[a]
dimers	0.0	0.0	2.5	0.05
fragmentation				
C_2H_2	52.2	1.14	52.5	0.93
M−H	4.6	0.05	16.7	0.17
recombination				
M + H	0.1	0.001	3.9	0.04
M + X ($10 < X < 100$ Da)	2.9	0.03	18.6	0.19

[a] Including dimers as two molecules.

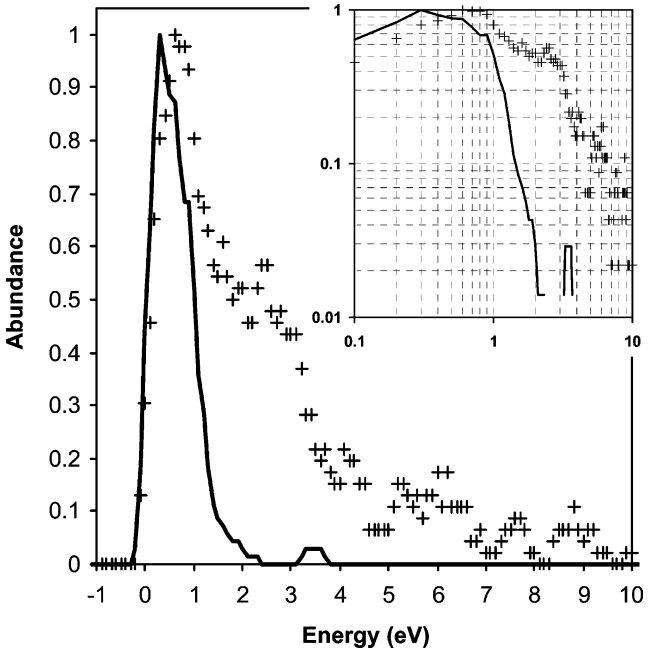

Figure 3. Calculated kinetic energy distributions of PS tetramers desorbed from sample B (solid line) and sample L (plus signs). Inset shows the same distributions in a log−log plot.

widths used for the data processing (2 eV in ref 34). As a corollary, the incident angle and the implementation of long-range forces in the MD code do not seem to have a strong influence on the calculated distributions for sample L. These energy spectra also reproduce the main features of the experimental KEDs of PS oligomers when adsorbed on silver, in particular, the high-energy tail extending beyond 5−10 eV.

However, the difference between the KEDs of PS molecules ejected from a bulk sample of polystyrene and from a molecular overlayer on silver is striking. The distribution corresponding to the bulk sample is almost symmetric: it peaks at 0.5 eV and does not extend beyond 2 eV. It covers only the low-energy portion of the energy spectrum of PS oligomers sputtered from a silver substrate. In turn, the high-energy tail, decaying as E^{-2} (beyond 2 eV) for the monolayer sample, follows an $E^{-4.5}$ power law (beyond 1 eV) for the bulk sample (see inset of Figure 3). These important differences mirror distinct emission processes, as is further investigated in the following subsection.

In contrast with the yield effect, the observation of narrower energy distributions for thicker organic samples is experimentally reported for all the systems considered in the literature. It is the case of neutral (post-ionized) benzene,[52] pyrenebutyric acid,[55] and phenol samples.[53] Notably, the same narrow energy distributions (peak below 1 eV, high-energy decrease as E^{-4}/E^{-5}) have also been observed for the keV Ar^+ ion-induced emission of molecular ions of glycerol,[56] poly(ethylene glycol),[57] and glycerol clusters.[56,57] Organic species desorbed not only from overlayers on metals under keV ion bombardment, but also from thick organic samples under MeV ion bombardment,[58−60] generally exhibit broader distributions with more-sustained high-energy tails. This prediction of the MD model should be further validated in future keV ion-induced sputtering experiments that involve samples composed of larger molecules such as our PS oligomers.

In our simulations, virtually all the ejected molecules originate from the surface layer (-5 Å $< z <$ 5 Å in Figure 2). It is quite different for small fragments. For instance, 26% of the acetylene fragments are emitted from deeper in the solid. Their depth of origin also has an influence on the kinetic energy: only 4% of those emitted from below $z = -5$ Å have a kinetic energy of >1 eV, versus 58% of those sputtered from the surface region (-5 Å $< z <$ 5 Å).

The simulation results provide more details concerning the manner the energy distributes within the ejected molecules. Figure 4 plots the kinetic energy as a function of the internal energy for the PS oligomers ejected from sample B (diamond-shaped symbols in Figure 4) and sample L (plus sign symbols in Figure 4). In both cases, most of the molecules have an internal energy between 0 eV and 40 eV. As a reminder from previous calculations, PS tetramers that have an internal energy of >30 eV are expected to decompose before reaching the detector in an analytical instrument such as the TRIFT Time-of-Flight SIMS (ULVAC−PHI).[34] Although the average internal energy is slightly higher for sample L, this difference is insignificant, in comparison to the observed kinetic energy spread (y-axis in Figure 4). The 500 eV Ar-ion bombardment of a bulk PS sample induces the emission of molecules with a much-higher ratio of internal energy versus kinetic energy than the bombardment of an overlayer of PS oligomers on silver. However, one cannot conclude that the Ar-ion-bombarded bulk PS samples are less efficient at desorbing stable intact molecules than PS-covered silver substrates, because the absolute internal energies are not larger, on average.

From the viewpoint of SIMS analysis, where ionization mechanisms determine the measured yields, the different electronic structures of the surfaces and the different average velocities (kinetic energies) calculated for the two configurations certainly constitute important parameters.

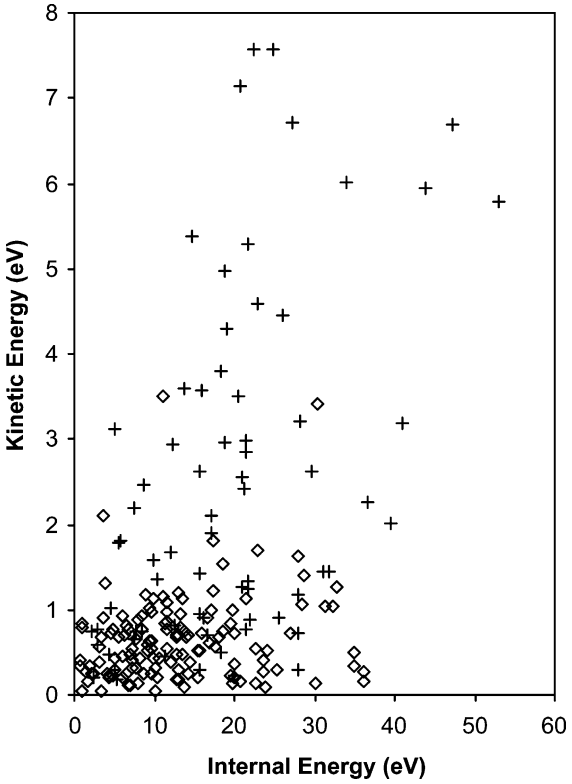

Figure 4. Plot of the kinetic versus internal energy of PS tetramers desorbed from (◇) sample B and (+) sample L.

3.3. Energy in the Surface Layer. Intrinsically, the MD simulation results provide a direct access to the time dependence of the ejection process (Figure 2) and the underlying energy-transfer mechanisms. To establish an understanding of these events, the chronology of the energy dissipation in the surface is investigated. For this purpose, the surface regions of both samples, i.e., above the dashed line in Figure 1b (sample B, -5 Å $< y <$ 5 Å in the scheme of Figure 2d) and above the *second* Ag atom layer in sample L (see ref 46), have been divided in squares with dimensions of 5 Å × 5 Å. The cumulated kinetic energy in each of these surface cells has been monitored as a function of time. Although there might be other definitions of the surface region as relevant as this one, our other attempts lead us, with more or less clarity, to similar observations as those presented hereafter. The evolutions of the kinetic energy in the surface are shown in Figure 5 (sample L) and Figure 6 (sample B) for typical trajectories ejecting three intact molecules. In these figures, a supplementary distinction is made between energy related to downward- (left frames) and upward-directed momenta (right frames). With this formalism, energy peaks that appear in the right frames should correlate with molecular desorption.

The situation at 61 fs for sample L reflects the partition of the projectile energy among a few energetic recoil atoms. After 272 fs, the energy is mostly localized in the vicinity of 4 (out of 13) molecules and the combination of the left and right frames indicates that the overall motion is markedly upward. There is some downward action happening between these molecules. Several cells have an energy of 10−15 eV, and many of them have an energy of 2−5 eV. Collective processes, indicated by the size of the energized region, continue to unfold after 446 fs but only zones 1−3 conserve an overall upward motion. After less than a picosecond, molecules 1−3 as well as a group of silver atoms have left the surface. The previously disturbed region has cooled and the energy per subunit cell is <1 eV,

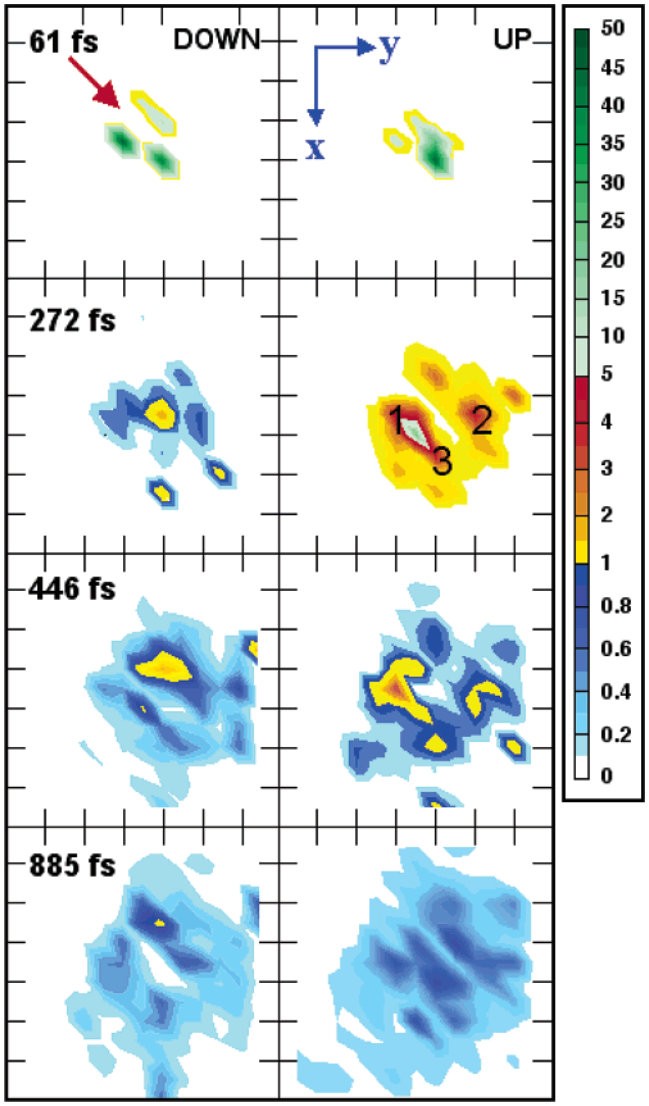

Figure 5. Time evolution (snapshots at 61, 272, 446, and 885 fs) of the kinetic energy distributed in the surface layer of sample L, for a trajectory inducing the ejection of three PS molecules. The left- and right-hand columns show the cumulated kinetic energy of atoms with a downward and upward momentum, respectively, in each 5 Å × 5 Å subcell of the surface layer (see text for details). The red arrow indicates the direction of the incoming projectile. The energy scale on the right-hand side of the figure is given in units of eV.

i.e., too low to induce further ejection. Note that the remaining energy is widely distributed, almost over the entire sample surface. For the record, the three PS oligomers sputtered in this trajectory have kinetic energies of 7.1, 1.8, and 0.9 eV.

The case considered in Figure 6 for sample B corresponds to the trajectory depicted in Figure 2. At 48 fs, only a few subunit cells are energized around the projectile impact point, while the collision cascade continues to develop deeper in the sample. The center of the surface area is gradually set in motion between 100 fs and 1 ps, with atoms of zone 1 clearly moving upward while the other areas display both upward and downward motion. Four picoseconds later, zone 1 is not colored anymore, indicating that the corresponding molecules and fragments (inset of Figure 2b) have left the surface region. At this point in time, the patterns are very similar in the right and left frames. The available energy is almost equally distributed in upward and downward motions in the excited molecules, which constitutes a clear signature of vibrational excitation. At 10 ps, there is still some localized action at the surface. The

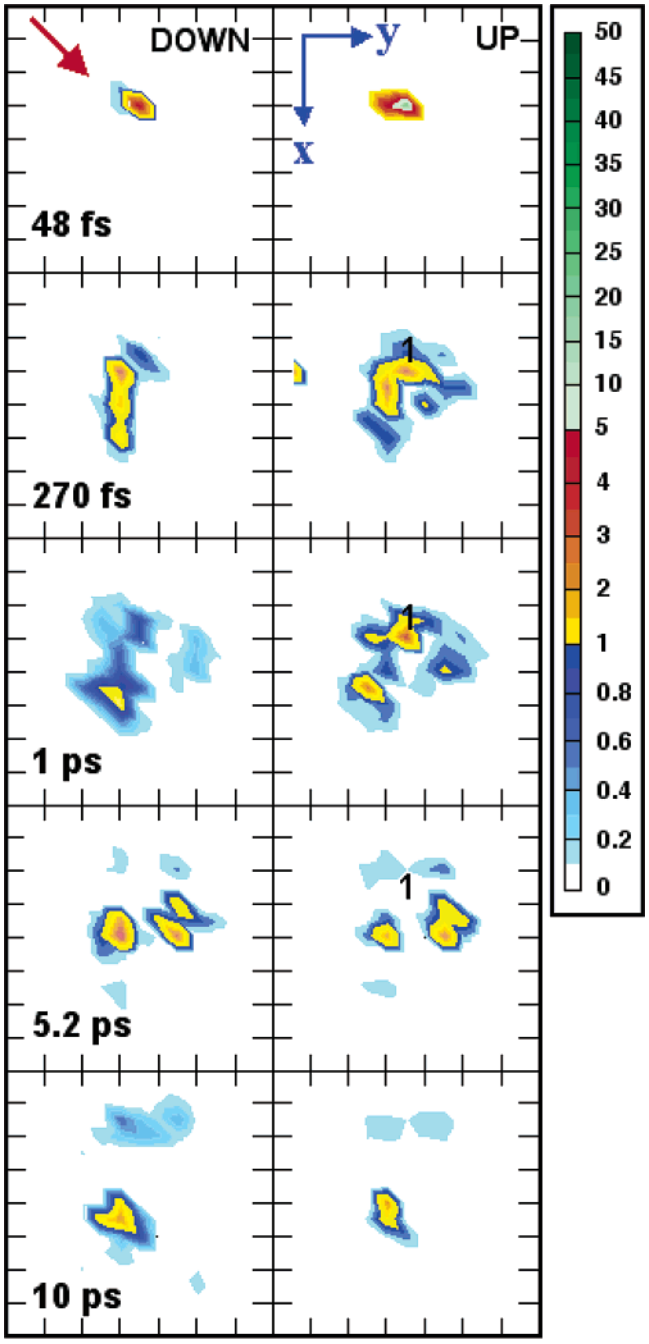

Figure 6. Time evolution (snapshots at 48 and 270 fs, and at 1.0, 5.2, and 10 ps) of the kinetic energy distributed in the surface layer of sample B, for a trajectory inducing the ejection of three intact PS molecules (same trajectory as Figure 2). The left- and right-hand columns show the cumulated kinetic energy of atoms with a downward and upward momentum, respectively, in each 5 Å × 5 Å subcell of the surface layer (see text for details). The red arrow indicates the direction of the incoming projectile. The energy scale on the right-hand side of the figure is given in units of eV.

last snapshot of Figure 2 shows that this remaining action is due to a molecule moving sideways, along the *x*-axis of the figures.

There are certainly two major differences in the manner of energy distribution in the surface of samples B and L. First, the energy-transfer process (as well as the emission) is much faster for molecules adsorbed on a silver substrate. The entire emission event proceeds within <1 ps, where ~10 ps are required for molecules to be ejected from a bulk PS sample. Second, the energy stored in the organic medium remains much more localized, especially after 500 fs. In contrast, the remaining energy becomes completely delocalized in the top silver layer of sample L between 500 fs and 1 ps. These differences are due to the various potentials at play. All the Ag atoms of sample L are equivalently linked to many neighbors via relatively strong and nondirectional bonds, which allows them to "communicate" quickly and efficiently, i.e., to distribute the projectile energy in the entire substrate (and among the adsorbed molecules) within a small amount of time. In addition, energy is more efficiently reflected toward the sample surface, because of the higher mass of Ag atoms, with respect to the mass of the projectile. In comparison, the PS solid is a network of soft, intermolecular bonds (a jelly) connecting groups of atoms linked by very strong, directional bonds (covalence). The vibration frequency mismatch between these two types of potentials manifests itself through a particularly weak energy coupling between separated molecules. In our opinion, the weakness of this coupling explains the comparatively slow energy transfer and pronounced energy localization observed in the surface region of sample B. It is also consistent with the more important internalization of energy, indicated by the similar right/left energy patterns of Figure 6 and the high ratios of internal energy versus kinetic energy of the ejected molecules (see Figure 4).

It is tempting to explain the lower average molecular yield observed for the overlayer sample (L) by the very fast dissipation of the projectile energy in the bulk of the metal substrate. (This interpretation was suggested by one reviewer of the article.) If the deposited energy can be quickly dissipated in the silver substrate of sample L, it can also be very efficiently reflected toward the surface in many instances (the trajectory of Figure 5 is a good example). Previous results obtained when comparing a free-standing and a silver-supported matrix:analyte sample even showed a positive effect of the metal substrate on the molecular emission yield.[33] Therefore, the reasons for the lower yield observed with sample L are complex, and we see at least four arguments that help explain the yield difference in our simulations: (i) The quantity of PS molecules in the surface layer (as defined previously) is ~4 times lower with the overlayer on metal (less material available); (ii) The binding energy of surface PS molecules is larger for the overlayer sample, which should limit the desorption yield; (iii) In many trajectories, the projectile channels across the crystalline silver substrate of sample L, without any induced molecular emission, which is less frequent with the amorphous organic sample; and (iv) The low mass of the projectile, with respect to the silver substrate, leads to a higher yield of projectile backscattering. In these cases, only a fraction of the energy is transferred to the surface atoms.

In contrast with self-supported benzene crystals[32] and benzene multilayers on metal under sub-keV projectile bombardment,[50] molecular collision cascades and "splash" effects are not clearly observed in our simulations. Thus, we believe that such behaviors are most probably a consequence of the small size and pronounced stiffness of benzene molecules, which allow them to behave, to some extent, similar to "super-atoms". PS oligomers, much like higher-mass polymers and biomolecules, have a long, flexible backbone with mobile—but linked—pendant groups. They form a somewhat entangled structure. This is certainly another reason explaining why, even departing PS molecules, which are expected to have the largest center of mass velocities in the sample, exhibit rovibrational energies that are 20 times larger (on average) than their translational energy.

3.4. Higher Projectile Energy and Secondary-Ion Mass Spectrometry Experiments. Current analytical instruments

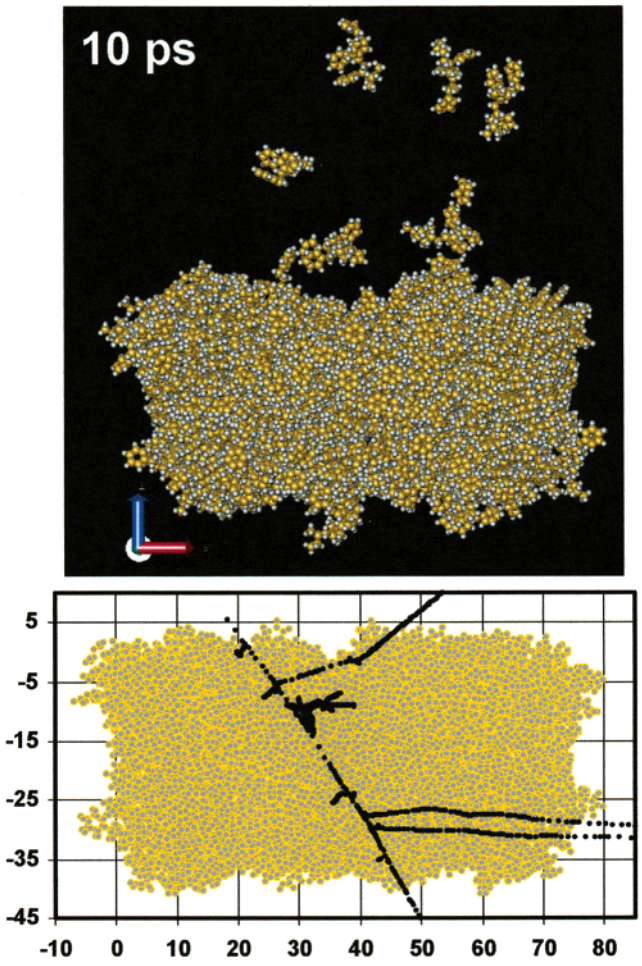

Figure 7. High-energy (5 keV) sputtering of sample B. Snapshot (10 ps) of the time evolution of a trajectory inducing molecular desorption with limited sample damage. The bottom frame of the figure shows the collision tree of the atomic collision cascade.

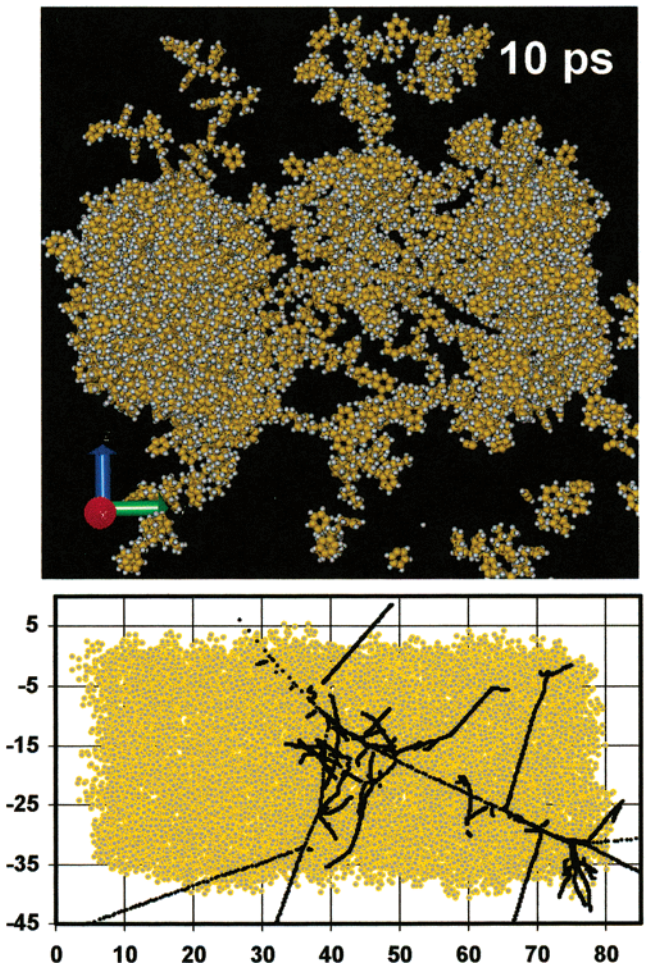

Figure 8. High-energy (5 keV) sputtering of sample B. Snapshot (10 ps) of the time evolution of a trajectory inducing molecular desorption with dramatic sample damage. The bottom frame of the figure shows the collision tree of the atomic collision cascade.

generally use primary particle sources, providing a beam of ions with energies in the range of 5−25 keV, i.e., approximately an order of magnitude larger than the previously considered projectile energy. Therefore, it also seemed important in the course of this study to grasp the essential differences induced by the use of significantly more energetic projectiles, although an in-depth analysis would require computer resources that are out of reach at this particular time. For this purpose, a series of trajectories was conducted using 5-keV Ar projectiles. Among the various collision cascade and sputtering events observed in these simulations, we present two extreme cases that lead to action at the surface and molecular ejection.

The first type of scenario is exemplified by the movie snapshot and the related collision tree of Figure 7. The side view of the sample at 10 ps shows a situation that seems qualitatively similar to that described in the low-energy trajectory of Figure 2. A group of PS molecules desorbs from the sample surface and, despite the much higher energy of the projectile, the sample keeps its integrity. The collision tree of the trajectory allows us to explain this unexpected result. It shows that the projectile crosses the solid with an almost straight trajectory, leaving by the bottom of the sample with a kinetic energy of 4.0 keV. On its way through the organic medium, it creates two energetic recoils leaving by the right side of the sample, ∼30 Å below the surface. In the more realistic case of a semi-infinite medium, with respect to the cascade volume, the projectile energy would be distributed deeper in the sample, via supplementary subcascades, whereas the two recoil atoms would probably create more action farther away from the impact point, in the buried layers of the sample. For this particular configuration, it is unlikely that additional molecular ejection would occur.

The trajectory depicted in Figure 8 constitutes another extreme case. In this event, our simulation cell is obviously too small to describe the sputtering process correctly. Indeed, the dissipation of the projectile energy causes the complete decomposition of the organic sample after 10 ps, with molecules and clusters being ejected in virtually all directions. Nevertheless, the analysis of such a trajectory provides us with interesting clues as to how a high action event unfolds in an organic solid under 5-keV bombardment. First, the way the collision cascade develops in the solid (bottom frame) should not be different with a larger sample. The dense network of subcascades observed in the center of our sample, involving a large number of bond scissions, might also cause a huge perturbation at the surface and eject a large amount of material if the organic medium were semi-infinite. Moreover, the projectile energy, relaxed in our system via the decomposition of the sample, would remain trapped in a larger sample, with no other choice than to dissipate through bond breaking, vibrational motion, or molecular ejection. A second important remark comes from the observation that the energy released in the organic medium (4.3 keV) causes the expansion/swelling of the sample in Figure 8. This expansion indicates the onset of a slow (but massive) cooperative molecular

motion in the bulk of the sample, after the collision cascade. In a semi-infinite sample, this effect might probably be sensed as a compression wave traveling away from the center of the excited volume.

From these examples, one may envision that the effect of the projectile energy, going from 500 eV to 5 keV, is to promote the occurrence of sputtering events where a larger volume of the sample is set in motion in a collective manner. An analogous effect had been foreseen in the case of PS molecules adsorbed on silver[34] and confirmed later on by running a larger set of trajectories.[46] The creation of an energized "track" in the sample (Figure 8) is reminiscent of MD simulations of keV atom impacts in metals[61,62] and rare gases,[21] as well as MeV ion irradiation of LJ solids.[26,63] The decomposition of the sample after energy dissipation has much in common with our own investigations of a smaller matrix:analyte sample under 500-eV Ar-ion bombardment.[33]

As mentioned previously, we do not know of any experiment where the yield of neutral PS molecules sputtered from a molecular sample was measured. In traditional SIMS experiments, PS oligomers are usually detected after their cationization by a metal atom, provided that the organic sample is deposited as a (sub)-monolayer on a clean metal substrate. Recently, it has been shown that the same effect could be obtained by evaporating a minute quantity of metal on top of a thick PS molecular film.[64] In such a situation, metal atoms are known to agglomerate, forming nanoclusters and islands on the surface. In ref 64, the observation of Au-cationized oligomers was interpreted as the result of the recombination of a departing molecule with a Au atom sputtered from a neighboring metal cluster in a single sputtering event. In the imparted time between metallization and analysis, the largest of these oligomers could not migrate on the metal clusters, excluding the possibility of a geometric configuration in which the molecules sit on top of a metal island. This experiment suggests that the interaction of a 15-keV projectile with a thick organic film is indeed able to induce dramatic ejection events, involving molecules and clusters. Although ions were measured, the same experiment also showed that the kinetic energy distributions of intact molecules were comparatively narrower when emitted from a thick film.[65]

4. Conclusion

The comparison between a thick sample made of polystyrene (PS) oligomers (sample B) and a monolayer of the same molecules physisorbed on silver (sample L) helped us identify the specifics of particle-induced desorption from a molecular solid. The statistical analysis of the trajectories shows that the molecular yield is higher with the bulk sample, in particular, PS molecular dimers are observed with a significant intensity. M−H and M + H sputtered species are, respectively, 4 and 30 times more intense with sample B, indicating that H-atom transfer is a very frequent process in thick organic sample sputtering. The average kinetic energy of the sputtered molecules is also comparatively lower, which seems to be in good agreement with the published experimental results concerning molecular solids. In this respect, the simulations provide a complementary piece of information, that is, the internal energy of the departing species is similar for both samples. As a consequence, the fraction of molecules undergoing unimolecular dissociation in the vacuum also should be the same. Our microscopic analysis of the energy transfer in the surface pinpoints two major differences between samples B and L: (i) the time scale of the energy dissipation/molecular ejection processes and (ii) the modalities of energy (de)localization in both samples. These differences are explained by the various potentials at play in the two systems. Because of the combination of stiff intramolecular bonds and soft intermolecular bonds, the energy transfer across the molecular sample surface is slow and a large fraction of the energy is stored in the vibrational modes of the excited molecules. As a result, the molecules are ejected at later times and with a lower ratio of kinetic energy versus internal energy. Finally, our results suggest that similar processes occur when the projectile energy is increased to 5 keV, although the chance of inducing large-scale, collective motion events at the surface is certainly larger.

Acknowledgment. The financial support of the National Science Foundation through the Chemistry Division is gratefully acknowledged by B.J.G. Additional computational resources were provided by the Academic Services and Emerging Technologies (ASET) of Penn State University. We are also indebted to the ASET staff for assistance with the Lion-xe and Lion-xl clusters.

References and Notes

(1) Garrison, B. J.; Delcorte, A.; Krantzman, K. D. *Acc. Chem. Res.* **2000**, *33*, 69.
(2) Garrison, B. J. In *ToF−SIMS: Surface Analysis by Mass Spectrometry*; Vickerman, J. C.; Briggs, D., Eds.; SurfaceSpectra/IMPublications: Manchester, U.K., 2001; p 223.
(3) Kerford, M.; Webb, R. P. *Nucl. Instrum. Methods Phys. Res., Sect. B* **2001**, *180*, 44.
(4) Smith, R.; Beardmore, K.; Gras-Marti, A.; Kirchner, R.; Webb, R. P. *Nucl. Instrum. Methods Phys. Res. B* **1995**, *102*, 211.
(5) *Appl. Surf. Sci.* **2003**, *203−204*, 1−879. (Proceedings of the XIIIth International Conference on Secondary Ion Mass Spectrometry, SIMS XIII.)
(6) Sigmund, P. In *Sputtering by Particle Bombardment I*; Behrisch, R., Ed.; Springer: Berlin, 1981; p 9.
(7) Sigmund, P. *Appl. Phys. Lett.* **1974**, *25*, 169.
(8) Sigmund, P.; Claussen, C. *J. Appl. Phys.* **1981**, *52*, 990.
(9) Kelly, R. *Radiat. Eff.* **1977**, *32*, 91.
(10) David, D. E.; Magnera, T. F.; Tian, R.; Stulik, D.; Michl, J. *Nucl. Instrum. Methods Phys. Res., Sect. B* **1986**, *14*, 378.
(11) Urbassek, H. M.; Michl, J. *Nucl. Instrum. Methods Phys. Res., Sect. B* **1987**, *22*, 480.
(12) Carter, G. *Radiat. Eff. Lett. Sect.* **1979**, *43*, 193.
(13) Carter, G. *Nucl. Instrum. Methods Phys. Res.* **1983**, *209/210*, 1.
(14) Bitenski, I. S.; Parilis, E. S. *Nucl. Instrum. Methods Phys. Res., Sect. B* **1987**, *21*, 26.
(15) Bitenski, I. S. *Nucl. Instrum. Methods Phys. Res., Sect. B* **1993**, *83*, 110.
(16) Mahoney, J. F.; Perel, J.; Lee, T. D.; Martino, P. A.; Williams, P. *J. Am. Soc. Mass Spectrom.* **1992**, *3*, 311.
(17) Johnson, R. E.; Sundqvist, B. U. R.; Hedin, A.; Fenyo, D. *Phys. Rev. B* **1989**, *40*, 49.
(18) Kitazoe, Y.; Yamamura, Y. *Radiat. Eff. Lett. Sect.* **1980**, *50*, 39.
(19) Yamamura, Y. *Nucl. Instrum. Methods Phys. Res.* **1982**, *194*, 515.
(20) Webb, R. P.; Harrison, D. E., Jr. *Appl. Phys. Lett.* **1981**, *39*, 311.
(21) Waldeer, K. T.; Urbassek, H. M. *Nucl. Instrum. Methods Phys. Res., Sect. B* **1993**, *73*, 14.
(22) Bitenski, I. S.; Barofsky, D. F. *Phys. Rev. B* **1997**, *56*, 13815.
(23) Wong, S. S.; Rollgen, F. W. *Nucl. Instrum. Methods Phys. Res., Sect. B* **1986**, *14*, 436.
(24) Sundqvist, B. U. R. *Nucl. Instrum. Methods Phys. Res., Sect. B* **1990**, *48*, 517.
(25) Reimann, C. T. *Nucl. Instrum. Methods Phys. Res., Sect. B* **1995**, *95*, 181.
(26) Fenyö, D.; Sundqvist, B. U. R.; Karlsson, B. R.; Johnson, R. E. *Phys. Rev. B* **1990**, *42*, 1895.
(27) Shiea, J. T.; Sunner, J. In *Methods and Mechanisms for Producing Ions from Large Molecules*; Standing, K. G.; Ens, W., Eds.; Plenum Press: New York, 1991; p 147.
(28) Williams, P.; Sundqvist, B. U. R. *Phys. Rev. Lett.* **1987**, *58*, 1031.
(29) Beardmore, K.; Smith, R. *Nucl. Instrum. Methods Phys. Res., Sect. B* **1995**, *102*, 223.
(30) Nordlund, K.; Salonen, E.; Keinonen, J.; Wu, C. H. *Nucl. Instrum. Methods Phys. Res., Sect. B* **2001**, *180*, 77.
(31) Stuart, S. J.; Tutein, A. B.; Harrison, J. A. *J. Chem. Phys.* **2000**, *112*, 6472.

(32) Krantzman, K. D.; Postawa, Z.; Garrison, B. J.; Winograd, N.; Stuart, S. J.; Harrison, J. A. *Nucl. Instrum. Methods Phys. Res., Sect. B* **2001**, *180*, 159.

(33) Delcorte, A.; Garrison, B. J. *J. Phys. Chem. B* **2003**, *107*, 2297.

(34) Delcorte, A.; Vanden Eynde, X.; Bertrand, P.; Vickerman, J. C.; Garrison, B. J. *J. Phys. Chem. B* **2000**, *104*, 2673.

(35) Krantzman, K. D.; Fenno, R.; Delcorte, A.; Garrison, B. J. *Nucl. Instrum. Methods Phys. Res., Sect. B* **2003**, *202*, 201.

(36) Chatterjee, R.; Postawa, Z.; Winograd, N.; Garrison, B. J. *J. Phys. Chem. B* **1999**, *103*, 151.

(37) Harrison, D. E., Jr. *CRC Crit. Rev. Solid State Mater. Sci.* **1988**, *14*, S1.

(38) Winograd, N.; Garrison, B. J. In *Ion Spectroscopies for Surface Analysis*; Czanderna, A. W., Hercules, D. M., Eds.; Plenum Press: New York, 1991; p 45.

(39) Brenner, D. W. *Phys. Rev. B* **1990**, *42*, 9458.

(40) Brenner, D. W.; Harrison, J. A.; White, C. T.; Colton, R. J. *Thin Solid Films* **1991**, *206*, 220.

(41) Brenner, D. W.; Shenderova, O. A.; Harrison, J. A.; Stuart, S. J.; Ni, B.; Sinnott, S. B. *J. Phys.: Condens. Matter* **2002**, *14*, 783.

(42) Kelchner, C. L.; Halstead, D. M.; Perkins, L. S.; Wallace, N. M.; DePristo, A. E. *Surf. Sci.* **1994**, *310*, 425.

(43) Biersack, J. P. In *Ion Beam Modification of Materials*; Mazzoldi, P.; Arnold, G. W., Eds.; Elsevier: Amsterdam, 1987; p 648.

(44) Information concerning this program can be found at the following Internet address: http://www.research.ibm.com/ion-beams/SRIM/.

(45) Garrison, B. J.; Kodali, P. B. S.; Srivastava, D. *Chem. Rev.* **1996**, *96*, 1327.

(46) Delcorte, A.; Garrison, B. J. *J. Phys. Chem. B* **2000**, *104*, 6785.

(47) Harrison, D. E., Jr.; Delaplain, C. B. *J. Appl. Phys.* **1976**, *47*, 2252.

(48) Wucher, A.; Garrison, B. J. *Phys. Rev. B* **1992**, *46*, 4855.

(49) Lias, S. G.; Bartmess, J. E.; Liebman, J. F.; Holmes, J. L.; Levin, R. D.; Mallard, W. G. *J. Phys. Chem. Ref. Data* **1988**, *17* (Suppl. 1).

(50) Postawa, Z.; Ludwig, K.; Piakowski, J.; Krantzman, K. D.; Winograd, N.; Garrison, B. J. *Nucl. Instrum. Methods, Sect. B* **2003**, *202*, 168.

(51) Mollers, R.; Schnieders, A.; Kortenbruck, G.; Benninghoven, A. In *Secondary Ion Mass Spectrometry, SIMS X*; Benninghoven, A., Hagenhoff, B., Werner, H., Eds.; Wiley: New York, 1997; p 943.

(52) Chatterjee, R.; Riederer, D. E.; Postawa, Z.; Winograd, N. *J. Phys. Chem. B* **1998**, *102*, 4176.

(53) Meserole, C. A.; Vandeweert, E.; Postawa, Z.; Haynie, B. C.; Winograd, N. *J. Phys. Chem. B* **2002**, *106*, 12929.

(54) Schnieders, A.; Schroder, M.; Stapel, D.; Arlinghaus, H. F.; Benninghoven, A. In *Secondary Ion Mass Spectrometry, SIMS XII*; Benninghoven, A., Bertrand, P., Migeon, H.-N., Werner, H., Eds.; Wiley: New York, 2000; p 263.

(55) Chatterjee, R.; Riederer, D. E.; Postawa, Z.; Winograd, N. *Rapid Commun. Mass Spectrom.* **1998**, *12*, 1226.

(56) Hoogerbrugge, R.; Van der Zande, W.; Kistemaker, P. G. *Int. J. Mass Spectrom. Ion Process.* **1987**, *76*, 239.

(57) Kelner, L.; Markey, S. P. *Int. J. Mass Spectrom. Ion Process.* **1984**, *59*, 157.

(58) Mosshamer, R. Ph.D. Thesis, Institute of Nuclear Physics, Technische Hoogschule Darmstad, 1985. (Reported in Betz, G.; Wien, K. *Int. J. Mass Spectrom. Ion Process.* **1994**, *140*, 1.)

(59) Zubarev, R. A.; Abeywarna, U.; Hakansson, P.; Demirev, P.; Sundqvist, B. U. R. *Rapid Commun. Mass Spectrom.* **1996**, *10*, 1966.

(60) Papaleo, R. M.; Demirev, P.; Eriksson, J.; Hakansson, P.; Sundqvist, B. U. R. *Phys. Rev. B* **1996**, *54*, 3173.

(61) Ghaly, M.; Averback, R. S. *Phys. Rev. Lett.* **1994**, *72*, 364.

(62) Postawa, Z.; Czerwinski, B.; Szewczyk, M.; Smiley, E. J.; Winograd, N.; Garrison, B. J. *Anal. Chem.* **2003**, *75*, 4402.

(63) Bringa, E. M.; Johnson, R. E. *Nucl. Instrum. Methods Phys. Res., Sect. B* **2002**, *193*, 365.

(64) Delcorte, A.; Médard, N.; Bertrand, P. *Anal. Chem.* **2002**, *74*, 4955.

(65) Delcorte, A.; Bour, J.; Aubriet, F.; Muller, J.-F.; Bertrand, P. *Anal. Chem.* **2003**, *75*, 6875.